International Journal of Scientific Research in Engineering and Management (IJSREM)
Volume: 10 Issue: 10 | Oct - 2026 SJIF Rating: 8.659 ISSN: 2582-3930

Static Structural Analysis and Gusset-Based Geometry Optimization of a Smartphone-Controlled Mini Electric Forklift

Dr.M.Dhande, Ansh Sharnagat, Moreshwar Daburkar, Sahil Kewat, Sanket Nikode, Shrunkhal Nitnaware, Sanket Chafle

Dr.M.S.Dhande: Assistant Professor, Department of Mechanical Engineering,
Priyadarshini College of Engineering, Nagpur, India
Other authors: B.Tech students, Department of Mechanical Engineering,
Priyadarshini College of Engineering, Nagpur, India
Corresponding author e-mail: mahendra.shivaji@gmail.com

Abstract—Miniature electric forklifts are ideally suited for workshop environments and educational laboratory facilities. However, their light metal frames are frequently designed intuitively, rather than analytically. This paper presents the static structural analysis of a smartphone controlled mini forklift based on an ESP32 controller, five 12 V geared DC motors and a belt-and-pulley lifting mechanism mounted on 12 mm guide rods. A SolidWorks Simulation model of the complete assembly was subjected to stepwise loads of 2.5 N to 20 N per fork arm, and three design variants were compared in terms of finite element method results: a bent L-bracket made of mild steel, the same bracket fabricated from alloy steel, and an alloy-steel box gusset plate. The mild-steel bracket exceeded its 250 MPa yield strength already at 2.5 N per arm (291.1 MPa). Utilization of alloy steel increased the allowable payload to approximately 1.1 kg with a factor of safety of 1.02 at 5.5 N per arm. Replacing the L-bracket by the gusset plate reduced the maximum von Mises stress at this load from 609.2 MPa to 168.8 MPa and the maximum deflection from 19.35 mm to 3.70 mm. The optimized frame can carry the 3 kg design payload with a factor of safety of 1.31 and yields at a mass of about 4 kg. The results of the simulation have not been compared to measurements on a prototype.

Keywords—Mini forklift, Static structural analysis, Finite element method, Gusset plate, Factor of safety, ESP32.

I. INTRODUCTION

Forklifts are among the most common machines for moving of goods in factories, warehouses and workshops. Conventional units are designed for pallet loads and large floor areas, and they have the cost, size and operator-training burden of heavy equipment. Laboratories, small workshops and teaching institutes often require something much smaller: a machine that can pick up a light box, carry it a few metres and put it

the paper reviews related work (Sec. II), describes the prototype and the simulation set-up (Sec. III), presents the results (Sec. IV), discusses their meaning and limits (Sec. V) and concludes (Sec. VI).

II. LITERATURE REVIEW

A. Electric and Small-Scale Forklifts

Electrification is the dominant theme in recent small-forklift work. Yadav et al. describe an electric forklift designed to lift to 1 ton to a height of 8 ft, in which a rechargeable battery and an electric motor replace the IC engine and the hydraulic lifting system [1]. Battery-operated and electric forklifts for small industrial warehouses and workshops are also treated by Sequeira et al. [2] and by Raut et al. [3], and Khebude reports the design and analysis of a mechanical forklift [5]. Cheng et al. modelled energy prediction and management of an electric forklift [9].

B. Remote and Smartphone Operation

Hema Latha et al. have developed a remotely controlled mini forklift bot and performed an analysis of selected parts subjected to loading in Ansys Workbench [6], while Jalal et al. have presented a low-cost mini forklift prototype which is controlled from a mobile phone via Bluetooth or Wi-Fi and performed Ansys structural analysis for a 50 N design load [7]. Thus, the technical literature confirms that mini forklifts controlled from remote locations or from a smartphone and structures subjected to analysis have been reported earlier. The prototype presented in this work follows similar concepts for control from a remote location using ESP32 microcontroller and a Bluetooth serial application.

C. Safety and Intelligent Functions

Lee et al. address the challenge of front-end failure of forklifts by means of predicting weight centers, the prediction of the remaining-useful-life under abnormal conditions and the diagnosis of failure based on alarm rules [4]. Shete et al. describe an ultrasonic blind-spot aid for of forklifts [8], Mohammadpour et al. study the energy-efficient motion planning of an autonomous forklift [10]. Obstacle sensing and autonomy are not part of the present prototype.

D. Research Gap

Considered jointly, these studies address electrification, remote operation, energy management and safety, and structural analysis of small forklifts, which has been reported in [6] and

[7]. Of the works reviewed here, the authors did not find a study that follows the increase in the stress and deflection of the load-carrying bracket as the payload is raised in steps towards yield, with the material and the joint geometry changed one at a time. This is a statement restricted to the works listed in this section, and no claim of novelty beyond them is made. The issue is of concern because it decides on the trustworthiness of a student-built forklift at its nameplate load. It is addressed in this paper with a load-stepped static analysis in which the material and geometry are changed one at a time.

III. METHODOLOGY

A. Requirements and Prototype

The forklift was designed for operating indoors on the floor at a lab or a small workshop, carrying light boxes and workpieces. Three requirements determined the design of the forklift. First, the forklift should be compact and light enough to be constructed from sheet and plate steel by students. Second, the forklift was designed to lift up a payload of 30 N (about 3 kg) by 30 cm. Finally, the forklift should be controlled from a safe distance without using a special transmitter.

The forklift is a four-wheel skid-steer vehicle with a front-mounted mast. The electronics are placed on a rigid base plate, including the wheel motors and a 12 V, 7 Ah sealed lead-acid battery. The battery is placed at the rear of the forklift to balance the load. The fork carriage is guided by linear slides made of two 12 mm rods and lifted by a belt-pulley mechanism driven by a 12 V, 60 RPM geared motor. The motor has two limit switches that control the movement of the forklift. The four-wheel vehicle uses four 12 V geared motors. The two motors at each side are connected in parallel to one of the channels of the L298N H-bridge. The turn of the vehicle is controlled by the rotation of the motors at different duty cycles, whereas the rotations of the motors at the two sides are opposite. The lift motor is controlled by two relays that reverse the polarity of the voltage on the motor. Fig. 1 below presents the design of the forklift.

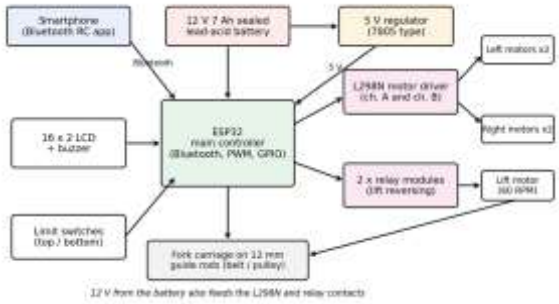


Fig. 1. Block diagram of the control system.

The ESP32 receives single-character commands from the Bluetooth RC Controller application on an Android phone via the built-in Bluetooth serial port and translates them into drive, speed and lift actions. The speed can be set in steps of 10 %. A 16 × 2 LCD and a buzzer give the status feedback to the operator. Three interlocks have been coded in the firm-ware: the two lift relays can never be energised together, the lift stops at a limit switch or after a 6 s run-time cut-off, and all motors stop if the Bluetooth link is lost. The program was written in the Arduino IDE. The vehicle is operated manually by the user from the phone and has no obstacle detection. Fig. 2(a) shows the SolidWorks model on which the structural study was set up, and Fig. 2(b) shows the fabricated prototype.

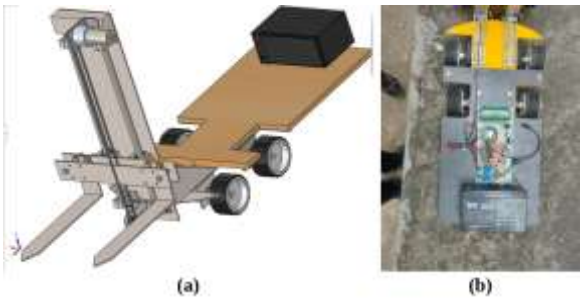


Fig. 2. (a) Isometric CAD model and (b) top view of the fabricated forklift.

B. Finite Element Model

1) Solver and Equations

The structural analysis was conducted in SOLIDWORKS Simulation Premium 2025 SP1.2 [11] on the complete assembled product model. The assembly consists of the wheels, the wheel motors, the upper lifting motor, the vertical mast plate, the wooden base plate, the fasteners and the bracket connecting the mast to the base, through which a linear static analysis was conducted, in which the nodal displacements {u} stem from the global stiffness matrix [K] and the load vector {F} through [12]

$$[K]\{u\} = \{F\} \qquad (1)$$

and the stress state is summarised by the von Mises equivalent stress [13]

$$\sigma_{vm} = \sqrt{\frac{1}{2}[(\sigma_1 - \sigma_2)^2 + (\sigma_2 - \sigma_3)^2 + (\sigma_3 - \sigma_1)^2]} \qquad (2)$$

2) Constraints, Loads and Mesh

The boundary conditions were kept identical in all the studies. A fixed support was applied on a circular face of the wheel and a roller/slider support on a rectangular face as indicated by Fig. 3(a). These hold the vehicle in an equilibrium on the floor line and leave it free to deflect. Two sets of a vertical point forces were applied as depicted in Fig. 3(b). One set was kept constant at 0.75 N per item while the magnitude of the other set that is, the payload per fork arm P was the study variable and was increased in steps from 2.5 N to 20 N. The forklift has two arms, and so total payload is 2P and the equivalent mass is

$$m = \frac{2P}{g} \qquad (3)$$

with g = 9.81 m/s². The design load of 30 N therefore corresponds to P = 15 N. The assembly was meshed with the automatic mesh generator of the program, and the mesh was inspected with the mesh-quality plot (Fig. 3(c)).

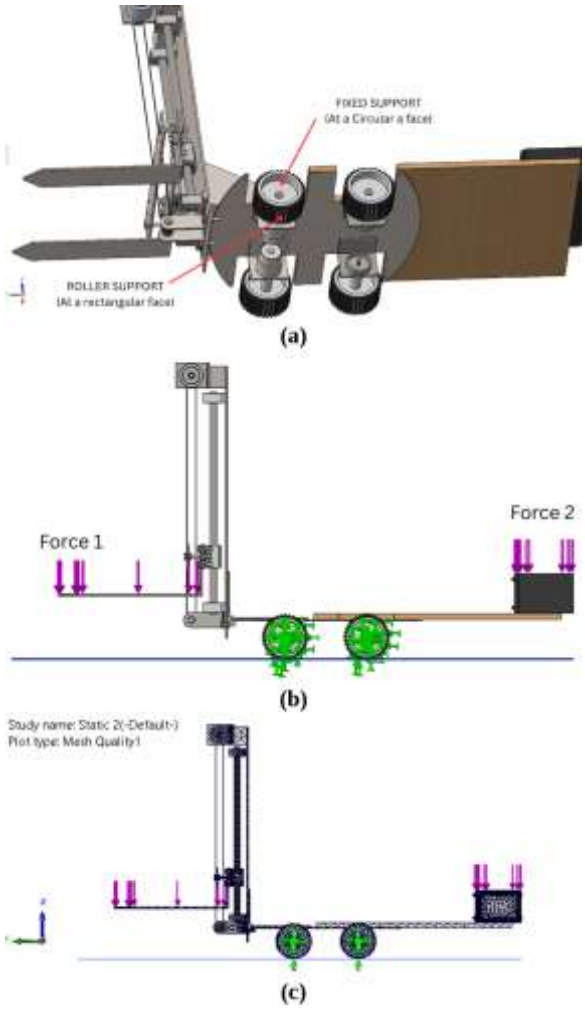


Fig. 3. Simulation set-up: (a) fixed and roller supports, (b) load sets, (c) mesh.

3) Materials and Evaluation Criteria

The library material properties were employed. The yield strengths on which the factors of safety are based are 250 MPa for mild steel and 620.4 MPa for alloy steel. The other components retained the materials assigned in the assembly model, for example, alloy steel for the vertical mast plate and balsa wood for the wooden base plate. The three results were read from each study: the maximum von Mises stress σ_max, the maximum resultant displacement δ_max, and the factor of safety.

$$FOS = \frac{\sigma_y}{\sigma_{max}} \qquad (4)$$

where σ_y is the yield strength of the material. A factor of safety below 1 means that the material yields. For a static check of a lifting device, a value of at least 1.5 was taken as the minimum acceptable.

C. Study Sequence and Geometry Optimization

Three configurations were studied and labeled C1, C2 and C3. C1 is the original bent L- bracket in mild steel, loaded at 2.5 N and 3 N per arm. C2 is the same bracket in alloy steel, loaded at 2.5 N, 4 N and 5.5 N per arm. C3 is the modified bracket in alloy steel, loaded at 5.5 N, 10 N, 15 N and 20 N per arm. The load was raised from one study to the next until the factor of safety dropped to about one, and the design was changed at that point.

The target set at the start was a capacity of at least 3 kg (15 N per arm) on the existing footprint, without a thicker plate or a heavy added structure, because the size and weight of the vehicle were limited. A change of material was tried first, as it needs no change to the fabrication process. When that proved insufficient, the geometry was changed. A solid gusset would stiffen the joint but would also add weight. Instead, two triangular side walls were added to the bracket, which turns the open L-section into a three-dimensional box-like gusset plate (Fig. 4). The side walls tie the vertical leg of the bracket to the horizontal leg along the line of the bending moment and add a stiff load path with little extra material.



Fig. 4. Original L-bracket (left) and the gusset plate with two triangular side walls (right).

D. Post-Processing

Because every study is linear, the peak stress is proportional to the load. A least-squares line through the origin was therefore fitted to the points of each configuration,

$$\sigma_{max} = kP \qquad (5)$$

and the payload permitted for a required factor of safety FOS_req follows as P_allow = σ_y / (FOS_req · k). The gain of the gusset plate over the L-bracket at equal load is expressed by the relative stress reduction

$$R = \frac{\sigma_L - \sigma_G}{\sigma_L} \times 100\% \qquad (6)$$

where σ_L and σ_G are the peak stresses of the L-bracket and of the gusset plate.

IV. RESULTS

Table I lists all nine simulated cases. The corresponding stress, displacement and factor-of-safety trends are plotted in Figs. 9 to 11.

TABLE I. RESULTS OF THE STATIC STUDIES

Case	P (N)	m (kg)	σmax (MPa)	δmax (mm)	FOS
C1	2.5	0.51	291.1	9.03	0.86
C1	3.0	0.61	332.5	11.05	0.75
C2	2.5	0.51	258.8	8.25	2.40
C2	4.0	0.82	434.0	13.80	1.43
C2	5.5	1.12	609.2	19.35	1.02
C3	5.5	1.12	168.8	3.70	3.68
C3	10	2.04	313.4	6.96	1.98
C3	15	3.06	474.0	10.58	1.31
C3	20	4.08	634.7	14.21	0.98

C1: mild-steel L-bracket (σy = 250 MPa). C2: alloy-steel L-bracket. C3: alloy-steel gusset plate (σy = 620.4 MPa for C2 and C3). P is the load per fork arm and m = 2P/g.

A. Mild-Steel L-Bracket (C1)

With the original bracket made of mild steel, the peak stress was 291.1 MPa (total payload 5 N (0.51 kg), 2.5 N per arm) which exceeds the 250 MPa yield strength, a factor of safety of 0.86 and would permanently deform under the first lifting. At 3 N per arm the peak stress increased to 332.5 MPa (Factor of safety 0.75) and the displacement of the mast top was 11.05 mm, Figure 5 showing the stress and displacement fields for the 3 N case. Most of the structure carries only a small fraction of the peak stress and the colour scale is dominated by a small region, suggesting that the bracket joint rather than the frame as a whole

dictates the capacity. Linear extrapolation suggests a yield load of this configuration of about 2.2 N per arm (0.45 kg)

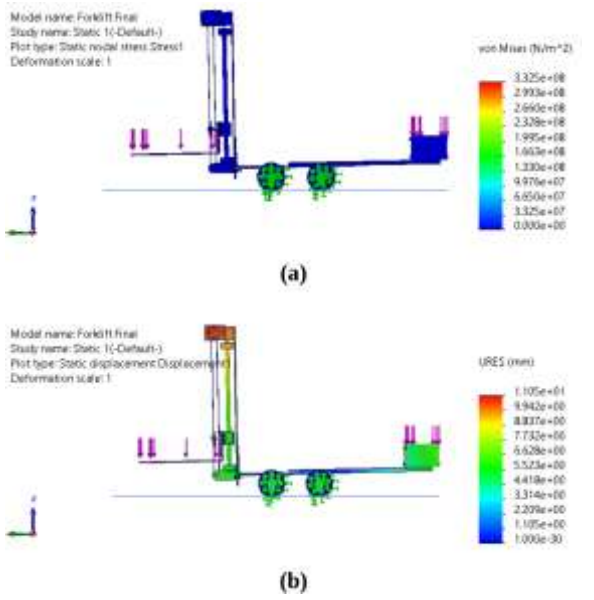


Fig. 5. C1 at 3 N per arm: (a) von Mises stress, maximum 332.5 MPa; (b) resultant displacement, maximum 11.05 mm.

B. Alloy-Steel L-Bracket (C2)

It is possible to see that by replacing mild steel with alloy steel in the same bracket, the capacity was raised considerably. For example, under the loading of 2.5 N per arm, the peak stress was 258.8 MPa with a displacement of 8.25 mm, a factor of safety of 2.40 and the bracket passed. At 4 N per arm, the stress increased to 434.0 MPa (displacement 13.80 mm, safety factor 1.43) which no longer allows a comfortable margin. At 5.5 N per arm, a total of 11 N or 1.12 kg, the stress reached 609.2 MPa and the displacement 19.35 mm, a safety factor of 1.02 (Fig. 6). The unmodified bracket in alloy steel therefore reaches its limit at about 1.1 kg, well short of the 3 kg target.

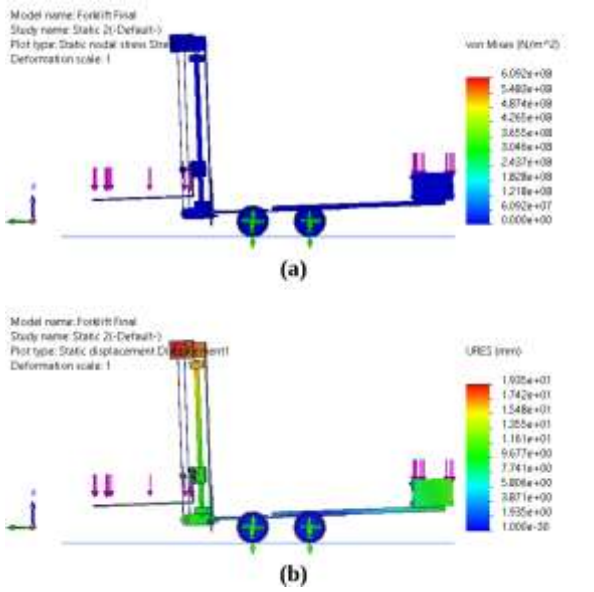


Fig. 6. C2 at 5.5 N per arm: (a) von Mises stress, maximum 609.2 MPa; (b) resultant displacement, maximum 19.35 mm.

C. Gusset Plate at Equal Load (C3)

With the gusset plate, the same load of 5.5 N per arm produced 168.8 MPa and 3.70 mm, a factor of safety of 3.68. Table II compares the two geometries at this load. The peak stress decreases by 72.3% and the peak displacement by 80.9%, resulting in an increase in the stiffness (load per arm divided by the peak displacement) by a factor of 5.2. A change that only affects the bracket reduced the peak stress by so much that it suggests that the bracket was the governing joint of the original design.

TABLE II. L-BRACKET AND GUSSET PLATE AT 5.5 N PER ARM

Quantity	C2	C3	Change
Peak von Mises stress (MPa)	609.2	168.8	−72.3 %
Peak displacement (mm)	19.35	3.70	−80.9 %
Factor of safety	1.02	3.68	× 3.6
Stiffness P/δ (N/mm)	0.28	1.49	× 5.2

D. Load Capacity of the Gusset Design

The gusset design was then further loaded. At 10 N per arm (2.04 kg) the peak stress was 313.4 MPa, the displacement 6.96 mm and the factor of safety 1.98. At 15 N per arm, which is the 30 N design load (3.06 kg), the peak stress was 474.0 MPa, the displacement 10.58 mm and the factor of safety 1.31 (Fig. 7). In the model the structure stays below yield at this load, so no permanent deformation is expected under static conditions. At 20 N per arm (4.08 kg) the peak stress was 634.7 MPa, above the 620.4 MPa yield strength, and the displacement was 14.21 mm. The factor of safety fell to 0.98 (Fig. 8), and this load marks the yield limit of the modelled structure.

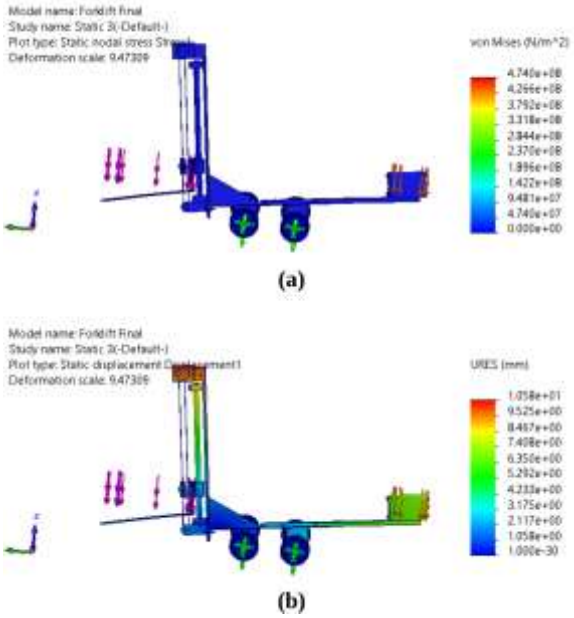


Fig. 7. C3 at 15 N per arm (design load): (a) von Mises stress, maximum 474.0 MPa; (b) resultant displacement, maximum 10.58 mm. Deformation scale 9.47×.

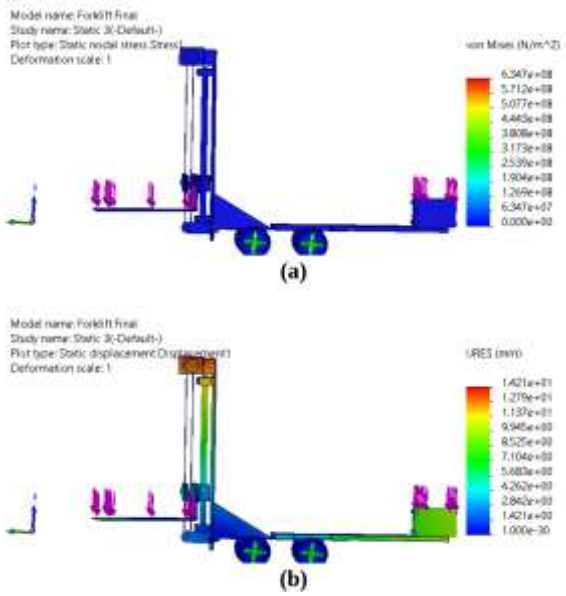


Fig. 8. C3 at 20 N per arm (yield limit): (a) von Mises stress, maximum 634.7 MPa; (b) resultant displacement, maximum 14.21 mm.

Figs. 9 and 10 show that stress and displacement increase approximately linearly with load for all three cases, as expected from a linear static analysis. The fitted slope of Eq. (5) was k = 31.6 MPa/N for the gusset plate and 109.2 MPa/N for the alloy-steel L-bracket and 113.1 MPa/N for the bracket in mild steel. Thus, with the same load produces about 3.5 times lower stress in the gusset plate than in the L-bracket made of the same steel. Table III gives the corresponding slopes converted into the masses that can be carried with the factor-of-safety of 1.0, 1.5, and 2.0. The gusset design carries about 4 kg at yield, 2.7 kg at a factor of safety of 1.5, and 2 kg at a factor of safety of 2. The values for the alloy-steel bracket are 1.16, 0.77, and 0.58 kg, respectively. The performance of the bracket made of mild steel is estimated based on two points only.

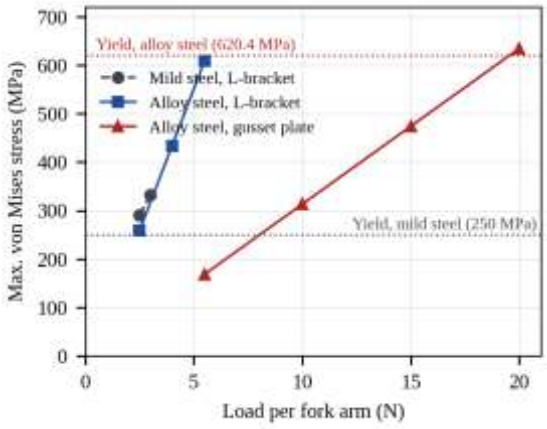


Fig. 9. Maximum von Mises stress against load per fork arm for the three configurations.

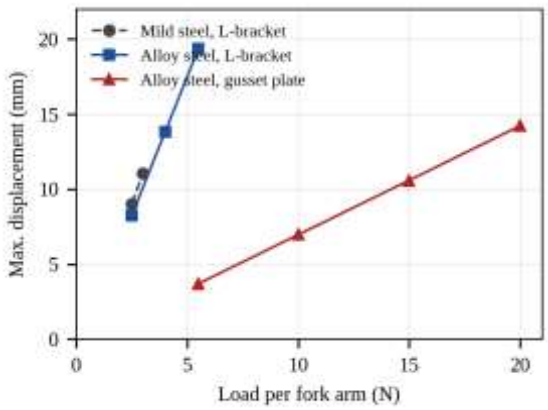


Fig. 10. Maximum resultant displacement against load per fork arm.

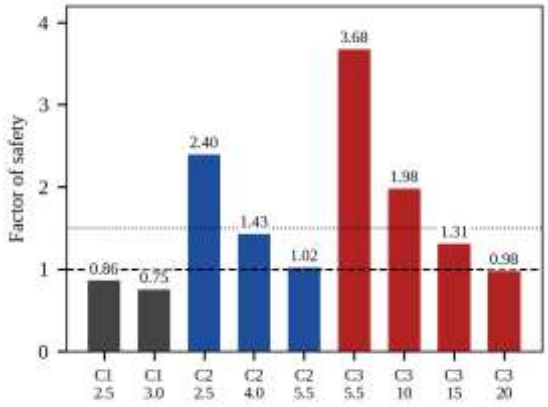


Fig. 11. Factor of safety of each simulated case (label: configuration and load per arm in N). The dashed line marks FOS = 1 and the dotted line FOS = 1.5.

TABLE III. PAYLOAD PERMITTED AT A REQUIRED FACTOR OF SAFETY

FOS_req	C1 (kg)	C2 (kg)	C3 (kg)
1.0	0.45	1.16	4.00
1.5	0.30	0.77	2.67
2.0	0.23	0.58	2.00

From P_allow = σ_y /(FOS_req · k) with the slopes k of Eq. (5); total payload m = 2P_allow/g.

E. Functional Behaviour of the Prototype

The only functional trials of the fabricated prototype were qualitative in nature. The vehicle was driven forward, backward and through turns on a flat floor with the speed changed from the application, and the carriage was raised and lowered from the application. These were observations only. No lifting time, load capacity, battery running time or Bluetooth range was measured, and no instrumented structural measurements were made, so the simulation results above are not supported by experiment.

V. DISCUSSION

A. Effect of Material and Geometry

Changing from mild steel into alloy steel increased the simulated yield load of the L-bracket by 2.6 times (from about 0.45 kg to 1.16 kg). This is close to the ratio of the two yield strengths, 620.4/250 = 2.5, which is to be expected for a stress-governed failure. The geometry change gave an additional increase of 3.5 times (from 1.16 kg to 4.0 kg). As these two factors combine (i.e., multiple), the final design then carries nine times the yield payload than the initial design. The geometry change was more significant than the change in the material, and it required neither a more expensive material nor a thicker plate.

The two changes also differ in their effect on the stiffness. Mild steel and alloy steel have almost the same elastic modulus, so that the displacement decreased only from 9.03 mm to 8.25 mm at 2.5 N per arm — a drop of 8.6 %. At the same load the peak stress also differs between the two steels (291.1 MPa against 258.8 MPa) although the geometry was the same. Peak values are local nodal values, so that this difference should be checked, for instance with a mesh-convergence study. The gusset plate reduced the displacement by 80.9 % at 5.5 N per arm. Only a change of shape can give this, and it explains why the deflection of the mast top is a more informative indicator than stress alone when a design is being improved.

B. Why the Gusset Plate Works

An open L-section is flexible in bending. Under the overturning moment of the payload the vertical leg rotates about the bend, and the bend itself carries the peak stress. Closing the corner with two triangular walls creates a box-like section whose second moment of area about the bending axis is much greater, with the addition of little material. The 5.2-fold increase in stiffness found in Table II is consistent with this explanation. The lower deflection also matters in use. A movement of 19 mm at the top of the mast, as with the L-bracket at 5.5 N per arm, would tilt the mast and the forks noticeably, whereas the gusset plate keeps it to 10.6 mm at the full design load of 30 N.

C. Rated Payload and Safety Margin

The factor of safety, of 1.31 at the 30 N design load, acceptable for a static check of a laboratory prototype is a thin margin to allow for the starting, stopping and lifting of a machine. The static analysis does not include the dynamic amplification due to starting and stopping the lift, the effect of rough floors or the effect of a load placed off-centre on the forks. On this basis and until the model is checked by measurement the authors suggest a rated payload of 2 kg (factor of safety of about 2.0) for routine use and 3 kg as the most that should be lifted with care on a flat floor. The yield limit at about 4 kg should be treated as a limit that is never approached, not as a capacity.

The 30 N design load is the same load as P = 15 N per arm in the structural study. The lift motor and the battery were not checked by calculation or by test in this work and should be verified before any payload rating is used

D. Limitations

Several limitations should be noted. Firstly, the study is linear and static. The dynamic effects due to repeated lifting and lowering and the transient accelerations due to starting and stopping are not included. A fatigue study is indicated, but no results are given. Secondly, the results have not been compared with measurements. Strain gauges on the bracket and a dial gauge on the top of the mast would give useful information about stresses. Thirdly, no mesh-convergence study is reported. Local loads such as point forces and supports can cause irregularities in the finite element solution, and peak values of nodal von Mises stress should be treated with caution. The quoted factors of safety should be examined in the context of the variation of these values. Fourthly, joint idealizations in the assembly affect the stresses. Lastly, the analysis is concerned only with the structure. The stability of the vehicle against tipping with the load raised was not investigated, even though the rear battery is positioned to provide a stabilizing moment. In addition, no calculations of a design nature were made for the lift drive, wheel motors, and battery, and the vehicle has no obstacle-avoidance sensors. Finally, the yield strengths are those of the library materials, and the actual properties of the plate stock used in fabrication could be different.

VI. CONCLUSION

A static structural simulation was performed on a smartphone-controlled mini electric forklift to determine whether its frame could withstand the 3 kg (30 N) payload that the lift drive was designed for. In the model, the original bent L-bracket in mild steel could not. It exceeded its yield strength at 2.5 N per arm, a payload of about half a kilogram. Alloy steel in the same bracket increased the usable payload to around 1.1 kg with a factor of safety of 1.02 at 5.5 N per arm. Adding two triangular side walls to form a box-like gusset plate reduced the peak von Mises stress at that load by 72.3% and the peak displacement by 80.9%. The improved design carries the 30 N design load with a factor of safety of 1.31 and a mast-top displacement of 10.58 mm, and reaches yield at about 20 N per arm, which is a total of roughly 4 kg.

The geometry change was more worthwhile than the change of material and did not require thicker plate, which keeps the vehicle light. Based on these simulation results, a rated payload of 2 kg (factor of safety about 2.0) is suggested for routine use. The main limitations of the work are its static and linear nature, the lack of experimental validation, of a reported mesh-convergence study and of design calculations for the drive, lift and battery, and the lack of a tipping-stability analysis. Future work therefore will cover strain-gauge and deflection measurements on the prototype, fatigue and dynamic analysis of the improved bracket, a tipping-stability study, and possible electronic additions such as obstacle detection, load sensing, battery monitoring and IoT-based supervision, none of which is present in the current vehicle

ACKNOWLEDGEMENT

The authors thank Dr. I. A. Khan, Head of the Department of Mechanical Engineering, Dr. S. A. Dhale, Principal, and Dr. G. M. Asutkar, Vice Principal, Priyadarshini College of Engineering, Nagpur, for the facilities and encouragement provided during this work.

REFERENCES

[1] J. Yadav, M. Vishwakarma, S. M. Shakir, S. Yadav and Y. Rehman, “Design and fabrication of electric forklift,” Int. J. Res. Appl. Sci. Eng. Technol. (IJRASET), vol. 10, no. 4, pp. 589–593, Apr. 2022, doi: 10.22214/ijraset.2022.41344.

[2] A. A. Sequeira, S. Mohammed, A. A. Kumar, M. Sameer, Y. A. Kareem, and K. H. Sachidananda, “Design and fabrication of battery-operated forklift,” J. Eur. Syst. Autom., vol. 52, no. 6, pp. 569–574, Dec. 2019, doi: 10.18280/jesa.520604.

[3] S. B. Raut, K. D. Gawade, V. N. Mane, S. N. More, and A. V. Suryavanshi, “Design of electric forklift used in small industrial warehouses and workshops,” Int. J. Eng. Res. Technol. (IJERT), vol. 9, no. 4, pp. 673–677, Apr. 2020.

[4] J.-G. Lee, Y.-S. Kim, and J. H. Lee, “Preventing forklift front-end failures: Predicting the weight centers of heavy objects, remaining useful life prediction under abnormal conditions, and failure diagnosis based on alarm rules,” Sensors, vol. 23, no. 18, Art. no. 7706, 2023, doi: 10.3390/s23187706.

[5] K. N. Khebude, “Design and analysis of mechanical forklift,” Int. J. Sci. Res. Eng. Dev. (IJSRED), vol. 3, no. 2, pp. 685–690, Mar.–Apr. 2020.

[6] K. Hema Latha, S. Misbahuddinhusaini, S. A. S. Sohail and M. A. Khan, “Design and analysis of a remotely operated mini forklift bot,” E3S Web Conf., vol. 309, Art. no. 01168, 2021, doi: 10.1051/e3sconf/202130901168.

[7] A. Jalal et al., “Design and development of a low-cost, eco-friendly forklift for sustainable logistics management,” Front. Built Environ., vol. 10, Art. no. 1506495, Jan. 2025, doi: 10.3389/fbuil.2024.1506495.

[8] R. G. Shete, S. K. Kakade, and M. Dhanvijay, "A blind-spot assistance for forklift using ultrasonic sensor," in Proc. IEEE Int. Conf. Technol., Res., Innov. Betterment Soc. (TRIBES), 2021, pp. 1–4, doi: 10.1109/TRIBES52498.2021.9751672.

[9] L. Cheng, D. Zhao, T. Li, and Y. Wang, "Modeling and simulation analysis of electric forklift energy prediction management," Energy Rep., vol. 8, pp. 353–365, 2022, doi: 10.1016/j.egyr.2022.03.071.

[10] M. Mohammadpour et al., "Energy-efficient motion planning of an autonomous forklift using deep neural networks and kinetic model," Expert Syst. Appl., vol. 237, part C, Art. no. 121623, Mar. 2024, doi: 10.1016/j.eswa.2023.121623.

[11] Dassault Systèmes, SOLIDWORKS Simulation Premium 2025 SP1.2, Vélizy-Villacoublay, France, 2025. [Software]. Available: https://solidworks.com

[12] O. C. Zienkiewicz, R. L. Taylor, and J. Z. Zhu, The Finite Element Method: Its Basis and Fundamentals, 7th ed. Oxford, U.K.: Butterworth-Heinemann, 2013.

[13] R. G. Budynas and J. K. Nisbett, Shigley's Mechanical Engineering Design, 10th ed. New York, NY, USA: McGraw-Hill, 2015.